Available online at www.sciencedirect.com

ScienceDirect

IFAC Papers Online CONFERENCE PAPER ARCHIVE

IFAC PapersOnLine 53-2 (2020) 12918–12923

Power Quality Management of Interconnected Microgrids using Model Predictive Control ⋆

F. Garcia-Torres * **S. Vazquez** ** **C. Bordons** ***
I. Moreno-Garcia **** **A. Gil** **** **P. Roncero-Sanchez** †

* *Centro Nacional del Hidrogeno, Puertollano (Ciudad Real), Spain, (e-mail: felix.garcia@cnh2.es).*
** *Electronic Engineering Department, Universidad de Sevilla, Sevilla, Spain, (e-mail: sergi@us.es)*
*** *Systems Engineering and Automatic Control Department, Universidad de Sevilla, Sevilla, Spain, (e-mail: bordons@us.es)*
**** *Department of Electronic and Computer Engineering, Universidad de Cordoba, Cordoba, Spain, (e-mail: isabel.moreno@uco.es)*
† *Systems Engineering and Automatic Control Department, University of Castilla-La Mancha, Ciudad Real, Spain, (e-mail: pedro.roncero@uclm.es)*

Abstract: In this paper, the power quality of interconnected microgrids is managed using a Model Predictive Control (MPC) methodology which manipulates the power converters of the microgrids in order to achieve the requirements. The control algorithm is developed for the microgrids working modes: grid-connected, islanded and interconnected. The results and simulations are also applied to the transition between the different working modes. In order to show the potential of the control algorithm a comparison study is carried out with classical Proportional-Integral Pulse Width Modulation (PI-PWM) based controllers. The proposed control algorithm not only improves the transient response in comparison with classical methods but also shows an optimal behavior in all the working modes, minimizing the harmonics content in current and voltage even with the presence of non-balanced and non-harmonic-free three-phase voltage and current systems.

Keywords: Interconnected systems, Harmonics, Predictive Control, Power System Control.

1. INTRODUCTION

Microgrids can be seen as a key technology to improve power quality and reliability (PQR). Their ability to work in grid-connected or islanded mode is specially adequate to supply electricity to sensitive loads. An introduction to the main problems and solutions of power quality in microgrids can be found in Guerrero et al. (2012). As can be seen in the aforementioned paper, most of the solutions for power electronics devices in microgrids are based on PI-PWM controllers which present slow transient response. Microgrids are not only electrical power systems essentially based on renewable energy systems but also they usually content sensitive loads to PQR losses. In environments with sensitive loads, fast response against problems related with PQR is required. MPC controllers are based on future behavior of the system, achieving fast dynamic response improving in this way the transient response of PI-PWM controllers, see Vazquez et al. (2016). Yazdi and Hosseinian (2019) introduce a novel Smart Branch to compensate power quality disturbances using a finite control set-model predictive controller (FCS-MPC). Jayachandran and Ravi (2019) present a decentralized model predictive hierarchical control strategy for islanded AC microgrids. An MPC controller is applied to the voltage control of an islanded microgrid in Garcia-Torres et al. (2015) for the case of non-linear loads. This method is expanded in Bordons et al. (2020) developing an MPC methodology to the cases of microgrids with non-linear and unbalanced loads in both grid-connected and islanded mode. The interconnection of microgrids can be considered as a way to increase the robustness in power supply overall when these microgrids have to work islanded from the main grid. This mode of operation of microgrids has hardly been studied to date.

In this paper, the work presented in Bordons et al. (2020) is expanded to be used in the case of interconnected microgrids working under a blackout of the main grid. The topology of the interconnected microgrids object of this paper is shown in Fig. 1. As can be seen in Fig. 1, there are three intelligent power switches (IPS) installed to isolate or connect the working mode of each microgrid with the main grid and/or with the neighbor microgrid.

⋆ This work has been partially supported by the Ministry of Economy and Competitiveness of Spain with the financial support under grant DPI2016-78338-R (Project CONFIGURA) and partially supported by Interreg SUDOE SOE3/P3/E0901 (Project IMPROVEMENT)

10.1016/j.ifacol.2020.12.2121

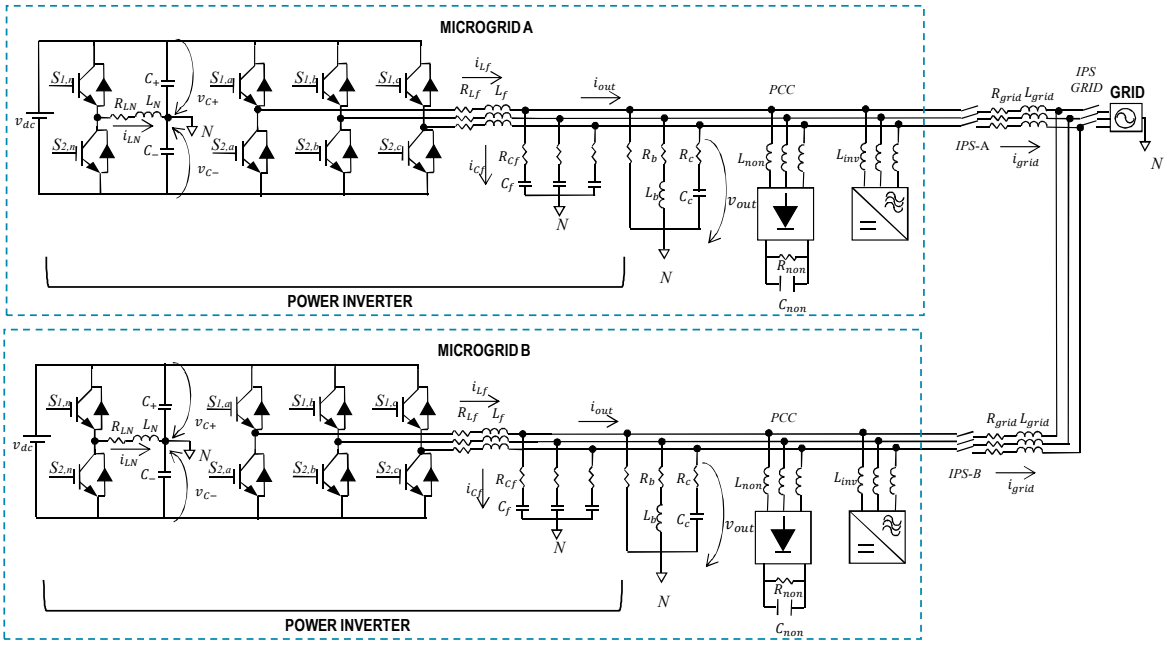

Fig. 1. Interconnected microgrids object of study

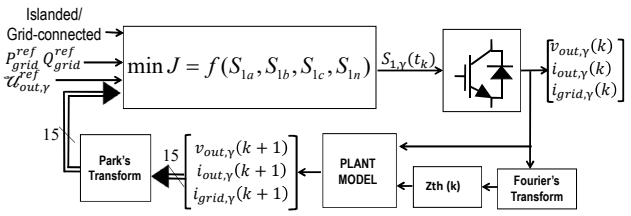

Fig. 2. Block Diagram

2. CONTROLLER DESIGN

In AC microgrids, the final power quality obtained in the microgrid depends on the exchanged power flow between its local devices connected and the grid. An appropriate energy storage system (ESS) connected to a voltage source inverter (VSI) can be used to enhance the power quality of the microgrid. The final result not only depends on the topology of the VSI but also on its control system. With the aim to obtain an optimal power flow in the microgrid, a four wire VSI with active neutral control is selected in order to integrate unbalanced and non-linear loads. The VSI response is improved using an innovative MPC controller to manage the power quality of the microgrids and their power exchange with the main grid or with the neighbor microgrids. The block diagram of the controller is exposed in Fig. 2. For the Park's transformation, it is considered that the d-axe is aligned with the voltage reference.

2.1 Predictive Model

The first step of the controller design is to calculate the equivalent output Thevenin's impedance at each sample instant $T_s$for every phase $Z^{th}_{out,\alpha}(k)|_{\alpha=a,b,c}$ for the fundamental frequency, using the phasors for output voltages $\mathscr{U}_{out,\alpha}$ and currents $\mathscr{I}_{out,\alpha}$:

$$Z^{th}_{out,\alpha}(k) = \frac{\mathscr{U}_{out,\alpha}(k)}{\mathscr{I}_{out,\alpha}(k) - \mathscr{I}_{grid,\alpha}(k)} = R^{th}_{out,\alpha}(k) + jX^{th}_{out,\alpha}(k) \quad (1)$$

An equivalent inductance or capacitance can be obtained. When $\text{sign}(X^{th}_{out,\alpha}(k)) = \text{sign}(R^{th}_{out,\alpha}(k))$ using relationship (2) and using the expression given in (3) when $\text{sign}(X^{th}_{out,\alpha}(k)) \neq \text{sign}(R^{th}_{out,\alpha}(k))$:

$$L^{th}_{out,\alpha}(k) = \frac{X^{th}_{out,\alpha}(k)}{2\pi f};\ C^{th}_{out,\alpha}(k) = 0 \quad (2)$$

$$L^{th}_{out,\alpha}(k) = 0;\ C^{th}_{out,\alpha}(k) = -X^{th}_{out,\alpha}(k) \cdot 2\pi f \quad (3)$$

The predictive model of the inverter as function of the switching vector $\mathbf{s}(k) = [S_{1a}(k)\ S_{1b}(k)\ S_{1c}(k)\ S_{1n}(k)]^T$ can be obtained with the expressions (4)-(6).

$$\begin{aligned} v_{out,\alpha}(k+1) &= V_{dc} \cdot (S_{1\alpha}(k+1) - S_{1n}(k+1)) \\ &+ \left(\frac{T_s R_{L_N} + L_N}{T_s}\right) \cdot i_{L_N}(k+1) - L_N \frac{i_{L_N}(k)}{T_s} \\ &- \left(\frac{T_s R_{L_{f\alpha}} + L_{f\alpha}}{T_s}\right) \cdot i_{L_{f\alpha}}(k+1) + L_{f\alpha} \frac{i_{L_{f\alpha}}(k)}{T_s}\Big|_{\alpha=a,b,c} \end{aligned} \quad (4)$$

$$\begin{aligned} i_{L_f,\alpha}(k+1) &= \frac{C_f}{T_s + C_f R_f} v_{out,\alpha}(k+1) \\ &\frac{T_s}{T_s R^{th,\mu grid}_{\alpha}(k) + L^{th,\mu grid}_{\alpha}(k)} v_{out,\alpha}(k+1) \\ &+ \frac{L^{th,\mu grid}_{\alpha}(k)}{T_s R^{th,\mu grid}_{\alpha}(k) + L^{th,\mu grid}_{\alpha}(k)} \cdot i_{out,\alpha}(k) \\ &- \frac{C_f}{T_s + C_f R_f} v_{out,\alpha}(k) + \frac{C_f R_f}{T_s + C_f R_f} i_{C_{f\alpha}}(k)\Big|_{\alpha=a,b,c} \end{aligned} \quad (5)$$

$$
\begin{aligned}
i_{L_N}(k+1) &= \left(1-\frac{2C_+}{T_s}\left(\frac{T_s R_{L_N}+L_N}{T_s}\right)\right)^{-1}\cdot \\
&\left(\sum_{\alpha=a,b,c}\frac{C_{f,\alpha}}{T_s}v_{C_f,\alpha}(k+1)+\frac{C_+}{T_s}V_{dc}\right. \\
&+\sum_{\alpha=a,b,c}\frac{T_s}{T_s R_\alpha^{th,\mu grid}(k)+L_\alpha^{th,\mu grid}(k)}v_{out,\alpha}(k+1) \\
&-\frac{C_+}{T_s}\left(v_{C+}(k)+v_{C-}(k)\right)-\sum_{\alpha=a,b,c}\frac{C_{f,\alpha}}{T_s}v_{C_f,\alpha}(k) \\
&\frac{L_\alpha^{th,\mu grid}(k)}{T_s R_\alpha^{th,\mu grid}(k)+L_\alpha^{th,\mu grid}(k)}\cdot i_{out,\alpha}(k) \\
&\left.-\frac{2C_+}{T_s}\left(L_N\frac{i_{L_N}(k)}{T_s}+V_{dc}\cdot S_{1n}(k+1)\right)\right)
\end{aligned}
\tag{6}
$$

In grid-connected mode the following equation has to be added:

$$
\begin{aligned}
&i_{grid,\alpha}(k+1) = L_{grid}i_{grid,\alpha}(k)+ \\
&\left.\frac{T_s}{R_{grid}T_s+L_{grid}}\left(v_{grid,\alpha}(k+1)-v_{out,\alpha}(k+1)\right)\right|_{\alpha=a,b,c}
\end{aligned}
\tag{7}
$$

2.2 Cost Function for the Islanded Mode

In this working mode the inverter object of this study has to manage the voltage waveform with respect to magnitude, frequency, harmonics content and phase equilibrium. In order to achieve these criteria, the cost function expressed in (8) is divided into three main parts: J_{isl}^{wave} which manages the waveform of the output voltage, J_{isl}^{harm} which minimizes the harmonics content and J_{isl}^{bal} which controls the balance between phases. In order to use the predictive model of the inverter, the assumption that between two sample instants $Z_{out,\alpha}^{th}(k+1) = Z_{out,\alpha}^{th}(k)$ has to be used in the predictive model of the inverter.

$$
\min_{\mathbf{s}(k)} J_{isl}(k) = \min_{\mathbf{s}(k)}\left(J_{isl}^{wave}(k)+J_{isl}^{harm}(k)+J_{isl}^{bal}(k)\right) \tag{8}
$$

$$
\begin{aligned}
J_{isl}^{wave}(k) = &\sum_{\alpha=a,b,c}\left[w_{isl}^{inst}\left(v_{out,\alpha}(k+1)-v_{out,\alpha}^{ref}(k+1)\right)^2\right. \\
&+w_{isl,\alpha}^{cycle}\left(\Re e(\mathscr{U}_{out,\alpha}(k+1))-\Re e(\mathscr{U}_{out,\alpha}^{ref}(k+1))\right)^2 \\
&\left.+w_{isl,\alpha}^{cycle}\left(\Im m(\mathscr{U}_{out,\alpha}(k+1))-\Im m(\mathscr{U}_{out,\alpha}^{ref}(k+1))\right)^2\right]
\end{aligned}
\tag{9}
$$

At each sample instant, the voltage reference is calculated and imposed in the first term of (9) minimizing the difference between the predicted voltage and the calculated reference. In order to minimize the steady-state error the second term of (9) is added, correcting this error with the complete fundamental cycle computation.

$$
\begin{aligned}
J_{isl}^{harm}(k) = &\sum_{\alpha=a,b,c}\left[w_{isl,\alpha}^{v}\left(\Delta v_{out,\alpha}(k+1)\right)^2\right. \\
&\left.+w_{isl,\alpha}^{i}\left(\Delta i_{out,\alpha}(k+1)\right)^2\right] \\
&+w_{isl}^{cap}\left(v_{C+}(k+1)-v_{C-}(k+1)\right)^2
\end{aligned}
\tag{10}
$$

The first and second term of (10) minimize the voltage and current abrupt variations between two sample instants avoiding the harmonics content in both voltage and current. The third term manages the balance of voltage for the neutral point.

$$
J_{isl}^{bal}(k) = \sum_{\alpha=a,b,c}^{\beta=b,c,a} w_{isl}^{bal}\left(|\mathscr{U}_{out,\alpha}(k+1))|-|\mathscr{U}_{out,\beta}(k+1)|\right)^2 \tag{11}
$$

When unbalanced loads are connected to the inverter the obtained voltage magnitude can take different values for each phase . In order to control these situations the term expressed in (11) is included in the cost function.

2.3 Cost Function for the Grid-Connected Mode

In grid connected mode, it is assumed that due to the fact that the voltage reference is imposed by the main grid. Under the assumption of robustness in the voltage waveform provided by the main grid and considering that Park's transformation is a rotational reference frame, it is considered that between two sample instants the *dqo*-voltage is constant. Under this assumption and using the predictive model can be obtained the output currents $i_{out,\gamma}(k+1)$ $i_{grid,\gamma}(k+1)$ of each phase.

The controller receives the set-point for the exchange of active and reactive powers with the main grid. Due to the fact that $\mathscr{U}_{grid,\alpha}^{ref}$ and $\varphi_{grid,\alpha}^{ref}$ are imposed by the main grid and supposed constant between two sample instants , it can easily obtained the reference current $\mathscr{I}_{grid,\alpha}^{ref}$ with the following equations:

$$
P_{grid,\alpha}^{ref}(k) = \frac{|\mathscr{U}_{grid,\alpha}^{ref}(k)||\mathscr{I}_{grid,\alpha}^{ref}(k)|}{2}\cos(\varphi_{grid,\alpha}^{ref}(k)) \tag{12}
$$

$$
Q_{grid,\alpha}^{ref}(k) = \frac{|\mathscr{U}_{grid,\alpha}^{ref}(k)||\mathscr{I}_{grid,\alpha}^{ref}(k)|}{2}\sin(\varphi_{grid,\alpha}^{ref}(k)) \tag{13}
$$

The current references are calculated as follows:

$$
\begin{aligned}
&i_{grid,\alpha}^{ref}(k+1) = \\
&|\mathscr{I}_{grid,\alpha}^{ref}(k+1)|\sin(2\pi f(k+1+D_\alpha)+\varphi_{grid,\alpha}^{ref}(k+1))
\end{aligned}
\tag{14}
$$

A digital delay D_α has to be included which is adaptive with $Z_{out,\alpha}^{th}(k)$. As done for the case of islanded mode, the cost function in grid-connected mode is divided into three parts:

$$
\min_{\mathbf{s}(k)} J_{conn}(k) = \min_{\mathbf{s}(k)}\left(J_{conn}^{wave}(k)+J_{conn}^{harm}(k)+J_{conn}^{bal}(k)\right) \tag{15}
$$

$$
\begin{aligned}
J_{conn}^{wave} = &\sum_{\alpha=a,b,c}\left[w_{conn}^{inst}\left(i_{grid,\alpha}(k+1)-i_{grid,\alpha}^{ref}(k+1)\right)^2\right. \\
&+w_{conn,\alpha}^{cycle}\left(\Re e(\mathscr{I}_{grid,\alpha}(k+1))-\Re e(\mathscr{I}_{grid,\alpha}^{ref}(k+1))\right)^2 \\
&\left.+w_{conn,\alpha}^{cycle}\left(\Im m(\mathscr{I}_{grid,\alpha}(k+1))-\Im m(\mathscr{I}_{grid,\alpha}^{ref}(k+1))\right)^2\right]
\end{aligned}
\tag{16}
$$

The procedure to formulate (16) is similar to the one carried out for (9). At each sample instant, the current reference is calculated and imposed in the first term of (16), minimizing the difference between the predicted current exchange with the main grid and the reference

calculated. In order to minimize the steady state error the second term of (16) is added correcting this error with the complete fundamental cycle calculus done for the current exchange with the main grid expressed in Fourier's domain.

$$J_{conn}^{harm}(k) = \sum_{\alpha=a,b,c} \Big[w_{conn,\alpha}^{v} \left(\Delta v_{out,\alpha}(k+1)\right)^2 + w_{conn,\alpha}^{i} \left(\Delta i_{grid,\alpha}(k+1)\right)^2 \Big] + w_{isl}^{cap} \left(v_{C+}(t_{k+1}) - v_{C-}(t_{k+1})\right)^2 \quad (17)$$

The second part of the cost function in grid-connected mode (17) minimizes the harmonic injection in current to the grid, as well as the voltage variations in the microgrid. It also balances the neutral point of the inverter. Finally, when unbalanced loads are connected to the microgrid they can affect to balance in the active and reactive power injected to main grid. For this purpose the term of the cost function expressed in (18) is included.

$$J_{conn}^{bal}(k) = \sum_{\alpha=a,b,c}^{\beta=b,c,a} w_{conn}^{bal}(P_{grid,\alpha}(k+1)) - P_{grid,\beta}(k+1)))^2 + \sum_{\alpha=a,b,c}^{\beta=b,c,a} w_{conn}^{bal}(Q_{grid,\alpha}(k+1)) - Q_{grid,\beta}(k+1)))^2 \quad (18)$$

2.4 Cost Function for the Interconnected Mode

The interconnected mode can be considered as a hybrid mode between the connected and the islanded mode since there does not exist a main grid who imposes the references in voltage and frequency but there can be energy exchange between the interconnected microgrids. Due to the fact that there is not a main grid both microgrids have to work controlling the voltage and the frequency, the so-called multi-master mode.

$$\min_{\mathbf{s}(k)} J_{inter}^{(X)}(k) = \min_{\mathbf{s}(k)} \Big(J_{isl}^{(X),wave}(k) + J_{isl}^{(X),harm}(k) + J_{isl}^{(X),bal}(k) + \sum_{\gamma=a,b,c} (i_{\gamma}^{(X)\to(Y)}(k))^2 \Big) \quad (19)$$

The notation (X) refers to the microgrids (A) and (B) and the terminology $(X) \to (Y)$ makes reference to the exchange between the microgrid (X) and the microgrid (Y), being $i_{(X)\to(Y)}^{exch}$ the exchanged current between the microgrid (X) and the microgrid (Y). Notice that this term achieves to syncronize in frequency both microgrids and also to equilibrate the voltage magnitude between both microgrids without being necessary any kind of communication between the interconnected microgrids.

3. SIMULATION RESULTS

The simulations are carried out using Simpower using $T = 1\mu s$ as sample period while the controller acts each $T = 20\mu s$. The different values for the simulation and power inverter components are exposed in Table 1.

Table 1. Components value

Parameter	Value
Filter inductance L_f	1 mH
Filter inductance resistance R_{L_f}	0.1 Ω
Filter capacitor C_f	0.5 mF
Filter capacitor resistance R_{C_f}	0.1 Ω
DC link voltage U_{dc}	950 V
Neutral inductance L_N	2.5 μ F
Neutral inductance resistance R_{L_N}	0.1 Ω
Neutral balancing capacitors C_+, C_-	6600 μF
Grid connection line inductance L_{grid}	0.1 mH
Grid connection line resistance R_{grid}	0.1 Ω
Slave inverter line inductance L_{inv}	0.1 mH
Slave inverter line resistance R_{inv}	0.1 Ω
Non-linear load line inductance L_{non}	0.1 mH
Non-linear load line resistance $R_{L_{non}}$	0.1 Ω
Non-linear load dc resistance R_{non}	60 Ω
Non-linear load dc capacitor C_{non}	6.6 mF
Unbalanced load phase a resistance R_a	1 MΩ
Unbalanced load phase b resistance R_b	10 Ω
Unbalanced load phase c resistance R_c	10 Ω
Unbalanced load phase b inductance L_b	1 mH
Unbalanced load phase c capacitor C_c	0.1 mF

3.1 Comparative between controllers

The first simulation is used to compare the results in both grid-connected and islanded mode, as well as the transition between modes using an MPC-controller and a PI-PWM-controller for a single microgrid working in both modes: grid-connected and islanded. In this simulation the non-linear and the unbalanced loads are connected to the microgrid in all the sample instants. Both controllers receive the next references for the power exchange with the main grid:

$$[P_{grid,\alpha}^{ref}, Q_{grid,\alpha}^{ref}] = [-15000 \text{ W}, -9000 \text{ Var}] \forall t \leq 0.5 \text{ s}$$
$$[P_{grid,\alpha}^{ref}, Q_{grid,\alpha}^{ref}] = [15000 \text{ W}, 9000 \text{ Var}] \forall t \geq 0.5 \text{ s}$$

Between $t \in [1s, 1.5s]$ a fault in the main grid occurs so the transition to islanded mode is required, restoring the connection of the microgrid with the main grid for $t > 1.5s$. The comparison between the results obtained in the reference tracking for the active and reactive power between the MPC and the PI controller can be found in Fig. 3. As can been seen in the figure, the PI controller presents a longer transient response while the MPC controller reaches the given references in just two cycles of the fundamental frequency. In Fig. 4, the comparison between the THD results for the MPC and PI controller are exposed. As can be seen, despite the presence of non-linear and unbalanced loads the current waveforms present a low content of harmonics in the MPC-controller while the PI controller is not able to minimize the harmonic content in the current waveform.

During the instants $t = 1$ s and $t = 1.5$ s, a grid blackout occurs and the power inverter works in islanded mode. The comparison between the behavior of the power inverter with the MPC and the PI-PWM controllers can be seen in Fig. 5 and Fig. 6 where the voltage magnitude and the phase values are shown. As it occurs for the case of grid-connected mode, a better transient response is obtained in the case of the MPC controller. A better response is also obtained for THD values of the voltage at the Point

of Common Coupling (PCC) in the case of the MPC controller as can be seen in Fig. 7.

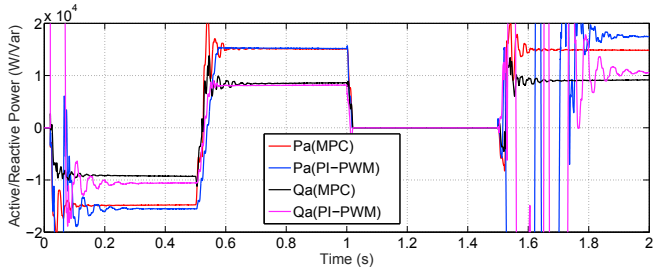

Fig. 3. Comparison of the results for the active and reactive power exchange with the main grid between the MPC and PI-PWM controllers for phase a

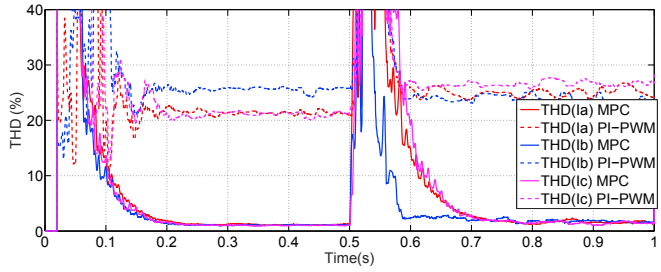

Fig. 4. Comparison of the THD values for the current exchange with the main grid between the MPC and PI-PWM Controllers

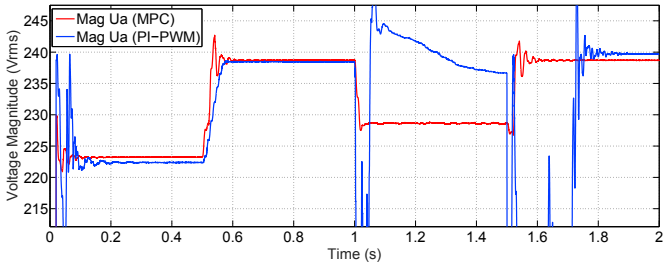

Fig. 5. Voltage Magnitude for phase A at the PCC

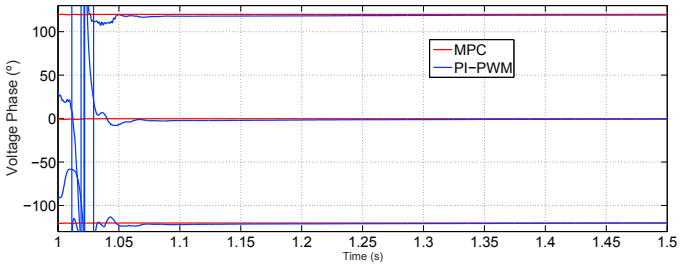

Fig. 6. Absolute voltage phase angle value of the voltages at the PCC during the blackout of the main grid

3.2 Power Quality Management Results for interconnected microgrids working without presence of grid

The aim of the second simulation launched is to evaluate the behavior of the presented controller for the case of interconnected microgrids working under a grid blackout.

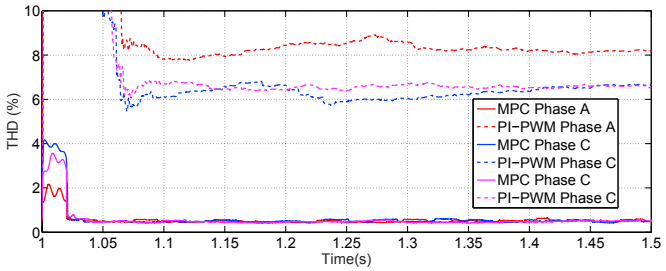

Fig. 7. THD values for the voltages at the PCC during the blackout of the main grid

In this case, the IPS-A and IPS-B are connected and IPS-grid is disconnected (see Fig. 1). In the case of the microgrid (A) the non-linear loads are connected during all the sample instants of the simulation and the unbalanced loads are connected for these sample instants $t > 0.1\ s$. In the microgrid (B) the unbalanced loads are connected during all the sample instants and the non-linear loads are connected at $t > 0.1\ s$. In Fig. 8 and Fig. 9 a comparison between the obtained results for the voltage magnitudes for every phase of each microgrid are shown. The current consumption can be observed in Fig.12. As can be seen, for the sample instants $t \in [0.10, 0.12]$ in Fig. 9 a more robust behavior is obtained in the case of working interconnected where the voltage magnitudes of each microgrids are always $|\mathscr{U}^{(X)}_{out,\gamma}| > 200$ for both microgrids. In Fig.13 the obtained results for the current exchange between both microgrids are shown. As can be seen, each microgrid manages its own loads without nearly non-affection to the neighbor microgrid. As can be seen in Fig. 10 and Fig. 11, the presence of non-linear and unbalanced loads and the changes in current demand at each microgrid, as well as the interaction between microgrids do not affect to the THD content in voltage or to the balance between phases guaranteeing the power quality supply to the loads connected to both microgrids.

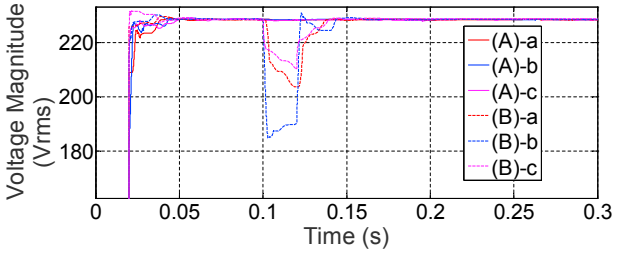

Fig. 8. Voltage Magnitude per phase and microgrid in mode non-interconnected and grid-islanded

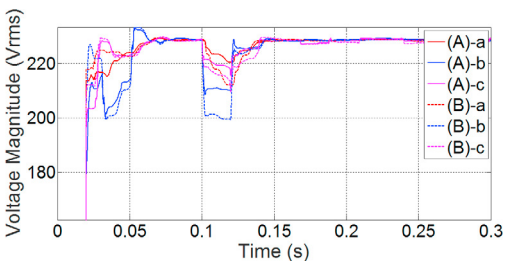

Fig. 9. Voltage Magnitude per phase and microgrid in mode interconnected and grid-islanded

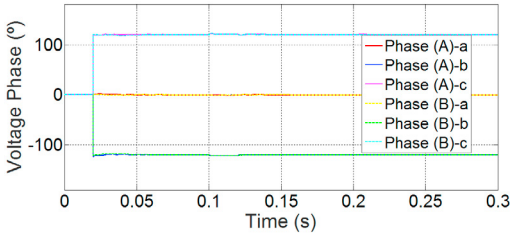

Fig. 10. Absolute voltage phase angle value per phase and microgrid in mode interconnected and grid-islanded

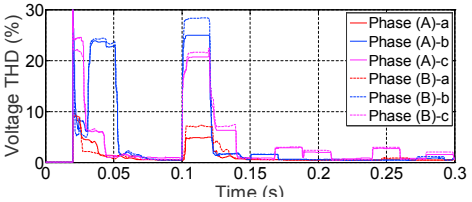

Fig. 11. Voltage THD per phase and microgrid in mode interconnected and grid-islanded

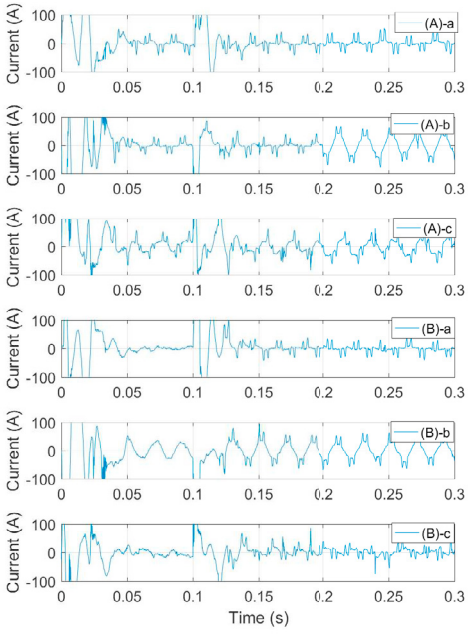

Fig. 12. Current per phase and microgrid in mode interconnected and grid-islanded

4. CONCLUSIONS

The main aim of the present study has been the implementation and validation under simulation of a methodology to manage the power quality in interconnected microgrids acting when they are grid-connected or under a grid blackout where they have to work interconnected but islanded from the main grid. The control algorithm is based on an MPC-controller applied to a four-wire three-phase VSI with active control of the neutral point which works as master of a microgrid with unbalanced and non-linear loads and generators connected. The simulation results show the potential of the presented MPC-controller in comparison wiht classical PI-PWM controllers solving the transient response problems of traditional methods. As can

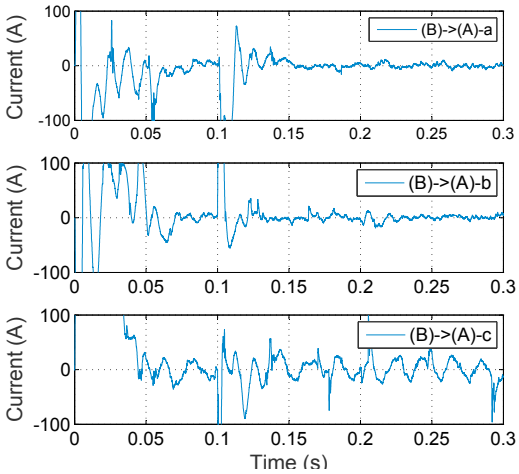

Fig. 13. Current exchange per phase between microgrid (A) and microgrid (B)

be seen, the developed methodology is improved with its application to the case of interconnected microgrids acting islanded from the main grid.

ACKNOWLEDGEMENTS

This work has been carried out with the financial support of the European Regional Development Fund (ERDF) under the program Interreg SUDOE SOE3/P3/E0901 (Project IMPROVEMENT) and the financial support by Spanish Ministry of Science, Innovation and Universities under grant DPI2016-78338-R (Project CONFIGURA).

REFERENCES

Bordons, C., Garcia-Torres, F., and Ridao, M.A. (2020). Model predictive control of microgrids.

Garcia-Torres, F., Bordons, C., and Vazquez, S. (2015). Voltage predictive control for microgrids in islanded mode based on fourier transform. In *2015 IEEE International Conference on Industrial Technology (ICIT)*, 2358–2363. IEEE.

Guerrero, J.M., Loh, P.C., Lee, T.L., and Chandorkar, M. (2012). Advanced control architectures for intelligent microgrids-part ii: Power quality, energy storage, and ac/dc microgrids. *IEEE Transactions on Industrial Electronics*, 60(4), 1263–1270.

Jayachandran, M. and Ravi, G. (2019). Decentralized model predictive hierarchical control strategy for islanded ac microgrids. *Electric Power Systems Research*, 170, 92–100.

Vazquez, S., Rodriguez, J., Rivera, M., Franquelo, L.G., and Norambuena, M. (2016). Model predictive control for power converters and drives: Advances and trends. *IEEE Transactions on Industrial Electronics*, 64(2), 935–947.

Yazdi, F. and Hosseinian, S. (2019). A novel smart branch for power quality improvement in microgrids. *International Journal of Electrical Power & Energy Systems*, 110, 161–170.